RNA (2001), *7*:661–670. Cambridge University Press. Printed in the USA.
Copyright © 2001 RNA Society.

The internal ribosome entry site (IRES) of hepatitis C virus visualized by electron microscopy

LUCY P. BEALES,[1] DAVID J. ROWLANDS,[1] and ANDREAS HOLZENBURG[2,3]

[1]School of Biochemistry and Molecular Biology, University of Leeds, Leeds LS2 9JT, United Kingdom
[2]School of Biology, University of Leeds, Leeds LS2 9JT, United Kingdom
[3]Electron Microscopy Center and Department of Biology, Texas A&M University, College Station, TX 77843-2257, USA

ABSTRACT

Translation of hepatitis C virus (HCV) RNA is initiated *via* the internal ribosome entry site (IRES), located within the 5′ untranslated region. Although the secondary structure of this element has been predicted, little information on the tertiary structure is available. Here we report the first structural characterization of the HCV IRES using electron microscopy. In vitro transcribed RNA appeared as particles with characteristic morphology and gold labeling using a specific oligonucleotide confirmed them to be HCV IRES. Dimerization of the IRES by hybridization with tandem repeat oligonucleotides allowed the identification of domain III and an assignment of domains II and IV to distinct regions within the molecule. Using immunogold labeling, the pyrimidine tract binding protein (PTB) was shown to bind to domain III. Structure–function relationships based on the flexible hinge between domains II and III are suggested. Finally, the architecture of the HCV IRES was seen to be markedly different from that of a picornavirus, foot-and-mouth disease virus (FMDV).

Keywords: electron microscopy; hepatitis C virus; internal ribosome entry site (IRES)

INTRODUCTION

In recent years, an increasing number of RNAs have been identified that initiate protein translation by a mechanism that is significantly different from the cap-binding/ribosome-scanning model (Kozak, 1989) typical for the majority of mRNAs. This alternative mechanism involves the direct binding of 40s ribosomal subunits to a region of complex secondary structure located upstream of the initiation codon, but downstream of the 5′ end of the mRNA. These internal ribosome entry sites (IRESs) are thus independent of a 5′ cap structure and many of the initiation factors associated with it. IRESs were first demonstrated within the 5′ untranslated region (UTR) of poliovirus (Pelletier & Sonenberg, 1988, 1989) and other picornaviral genomes (Jang et al., 1988, 1989; Belsham & Brangwyn, 1990; Glass et al., 1993). Subsequently, other viral genomes, such as those of pestiviruses (Poole et al., 1995), and a small number of eukaryotic mRNAs (Macejack & Sarnow, 1991; Vagner et al., 1995) have been shown to be translated by internal ribosomal entry.

The ability of a structured segment of RNA to direct translation in a cap-independent manner may be conclusively demonstrated by translation of dicistronic constructs in which the putative IRES is placed in the intercistronic space between two different reporter genes (Kaminski et al., 1994). The downstream reporter gene can only be translated if IRES activity is present. Using this approach, an IRES was identified within the 5′ UTR of the HCV genome (Tsukiyama et al., 1992) and the minimal sequence requirement for HCV IRES function has been mapped to the region between nt 40–341 (Honda et al., 1999b). However, sequences both up and downstream of the IRES appear to play a role in the control of initiation of translation (Reynolds et al., 1995; Rijnbrand et al., 1995).

The structure of the HCV IRES, as predicted from computerized analysis of the sequence, is supported by mutational analysis, ribonuclease mapping, and phylogenetic comparison (Fig. 1). The resulting well-characterized secondary structure model for HCV (Brown et al., 1992; Smith et al., 1995; Honda et al., 1996, 1999a) differs significantly from the predicted models of picornavirus IRESs. However, there is a high

Reprint requests to: Lucy P. Beales, Department of Microbiology, School of Biochemistry and Molecular Biology, University of Leeds, Old Medical School, Thoresby Place, Leeds LS2 9JT, United Kingdom; e-mail: l.p.beales@bmb.leeds.ac.uk.

Abbreviations: FMDV: foot-and-mouth disease virus; HCV: hepatitis C virus; IRES: internal ribosome entry site; PTB: polypyrimidine tract binding protein.

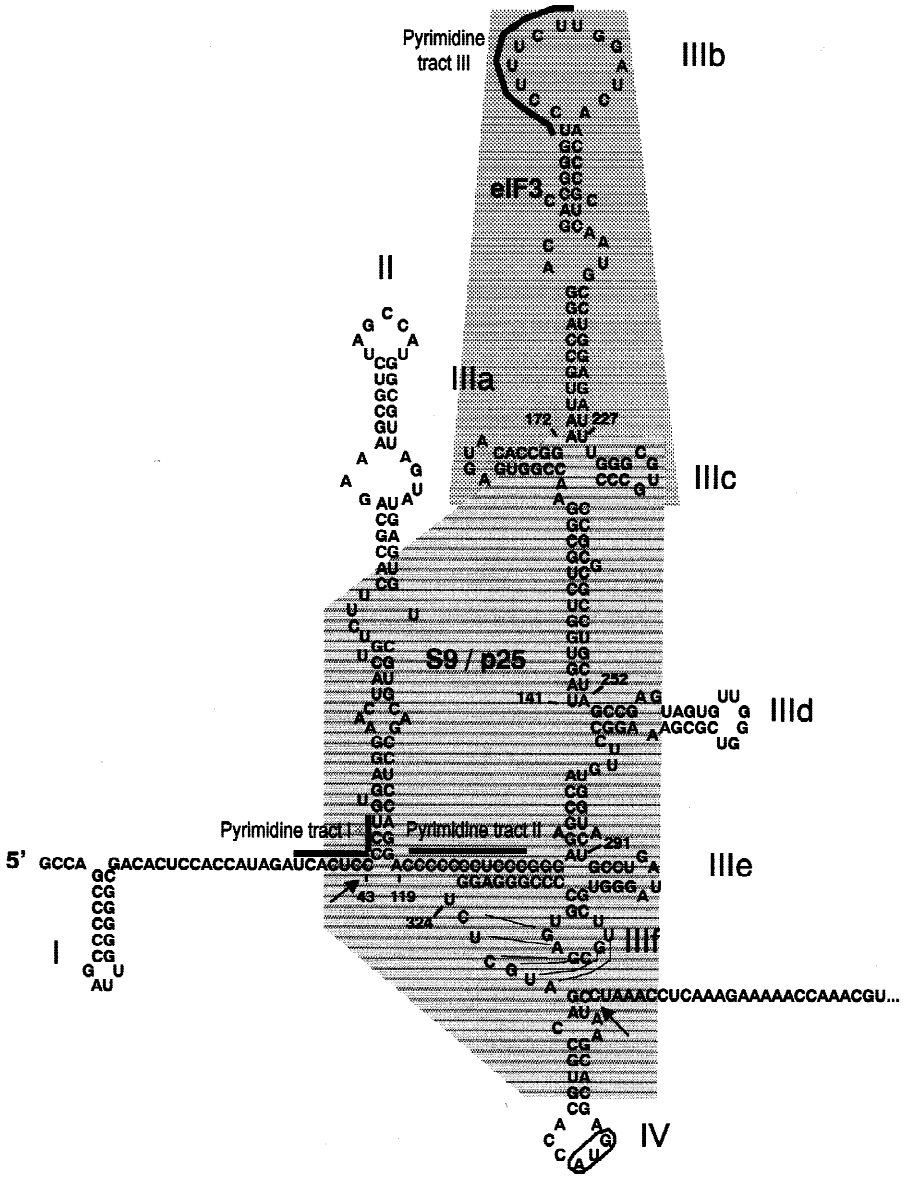

FIGURE 1. Proposed secondary and tertiary structure of the HCV 5′UTR (adapted from Honda et al., 1999a). Arrows represent the start and end of the minimal sequence required for efficient initiation of translation. Mapped binding sites for eIF3 and p25/S9 by block and lined shading, respectively.

degree of structural homology between the hepacivirus and pestivirus IRES elements despite the low level of sequence homology. The recognition motifs and functioning of the flavivirus IRES elements may therefore differ in significant details from those of the picornaviruses. Assembly of the translation machinery at the HCV IRES requires only eIF2 and eIF3 and no other host cell proteins (Pestova et al., 1998). This is in contrast to the mechanism of translation initiation seen with picornaviruses, which requires many of the canonical initiation factors necessary for cap-dependent initiation (Pestova et al., 1996). However, the interaction of eIF4F with picornaviral IRES elements occurs directly via the cleaved eIF4G subunit, or proteolytically derived fragment thereof, rather than the cap-binding eIF4E. Two noncanonical initiation factors are also involved in picornaviral initiation of translation. Polypyrimidine tract binding protein (PTB), a 57-kDa protein involved in RNA splicing, is necessary for efficient internal initiation of translation in several picornaviruses, including foot-and-mouth disease virus (FMDV; Borman et al., 1993; Hellen et al., 1993; Borvjagin et al., 1994; Kaminski et al., 1995; Niepman et al., 1997). The La autoantigen, a 52-kDa dsRNA unwinding enzyme, increases the activity of the poliovirus IRES (Meerovitch et al., 1989, 1993). Although there is no absolute requirement for these two proteins in HCV IRES-mediated translation, it has been shown that both PTB

(Ali & Siddiqui, 1995) and La (Ali & Siddiqui, 1997) bind to the IRES. Association of the 40s ribosomal subunit appears to occur by interaction of the S9 protein with motifs involving domains II and III (Fukushi et al., 1997; Sizova et al., 1998). The apical loop of domain III may also mediate in positioning of the 40s ribosomal subunit, as it has sequence complementarity to 18s rRNA.

The relationship between secondary and tertiary structure of the HCV IRES and its function has recently been established (Kieft et al., 1999). Correct folding, as demonstrated by small-angle X-ray scattering and chemical and enzymatic probing, was shown to be essential for IRES function. It was also demonstrated that at physiological salt concentrations, the HCV IRES adopts a unique, active conformation in the absence of the factors required for initiation of translation. Further biophysical analysis is required to confirm the proposed model and elucidate the three-dimensional structure of this and other IRESs. Internal ribosomal entry represents a possible target for antiviral therapy and detailed structural information would be of great value for the realization of this potential.

The three-dimensional structure of only a small number of RNA elements has been determined at atomic resolution. X-ray crystallography was first applied to the naturally abundant tRNA molecules (Kim et al., 1974; Robertus et al., 1974) and then to small, chemically synthesized RNA domains (Wahl & Sundaralingam, 1995). The ability to transcribe large quantities of RNA by in vitro transcription has recently made possible the crystallization of larger RNA structures such as ribozymes. A substantial increase in the understanding of RNA structure has been gained from the high-resolution ribosome structures recently published (Ban et al., 2000; Nissen et al., 2000; Schluenzen et al., 2000). However, these RNAs are components of large ribonuclear protein complexes rather than functioning as naked RNA. IRES elements on the other hand, comprising 300–600 nt, are significantly larger than the biggest RNA structure to be determined to date, that of the 160-nt *Tetrahymena thermophila* ribozyme (Cate et al., 1996). It is likely that they will prove difficult to crystallize in their entirety and resolution of the structure may be problematical. Thus, alternative approaches that provide low resolution maps of IRESs on which to superimpose high resolution data from X-ray crystallography and cryoelectron microscopy of specific domains will be useful steps en route to determining the completed structure of such large RNA molecules.

Electron microscopy (EM) is a well-established method for studying biomolecular assemblies and has been successfully used to retrieve high-resolution structural data for proteins (e.g., Chiu et al., 1998; Haley et al., 2000). The adaptation of such methods to the study of large RNA elements provides an attractive way forward. A combination of electron microscopic with X-ray crystallographic data will help to determine the entire three-dimensional RNA structure. Here we present for the first time electron microscopic studies of the HCV IRES and compare its observed structure with that of the IRES of a picornavirus, FMDV.

RESULTS

Visualization the HCV IRES

Examination of the transcribed HCV IRES RNA (Fig. 2A) by transmission electron microscopy, following negative staining with uranyl acetate, revealed distinctive particles comprising three “stems” protruding from a central axis (Fig. 3A). The largest stem (a) consistently measured 18 nm when compared to a calibrating reference grid. A smaller stem (b) of approximately 10 nm could be seen at various angles to the major stem. Measurements of 100 images showed the rotation between stems a and b to range from 70° to 130°, with a mean of 95° (Fig. 3B). The shortest stem (stem c) was just 2 nm and in some orientations it appeared to be obscured by the larger stems.

Confirmation of IRES identity

Gold labeling via a biotinylated oligonucleotide, complementary to the loop region of domain IIIb, was used to confirm that the structures seen by electron microscopy were, indeed, HCV IRES transcripts. The colloidal gold particles appeared as dense circular masses sur-

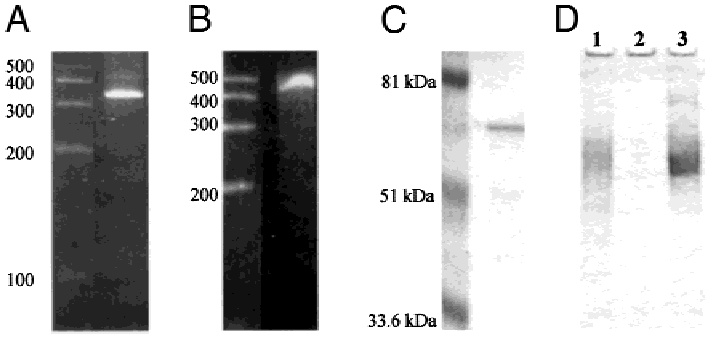

FIGURE 2. PAGE analysis of IRES RNA and PTB. **A,B:** Ethidium bromide-stained 6% polyacrylamide, 7 M Urea, TBE gels showing IRES RNA transcribed in vitro. **A:** HCV 5′UTR nt 1–380. **B:** FMDV IRES RNA. **C:** Purified His-PTB expressed in *E. coli* analyzed on a 12% polyacrylamide, SDS gel stained with Coomassie blue. **D:** Depletion of HCV IRES by coimmunoprecipitation with PTB. Samples analyzed on a 6% polyacrylamide, TBE gel stained with methylene blue; lane 1: HCV IRES alone; lane 2: HCV IRES with PTB; lane 3: HCV IRES with NS5A.

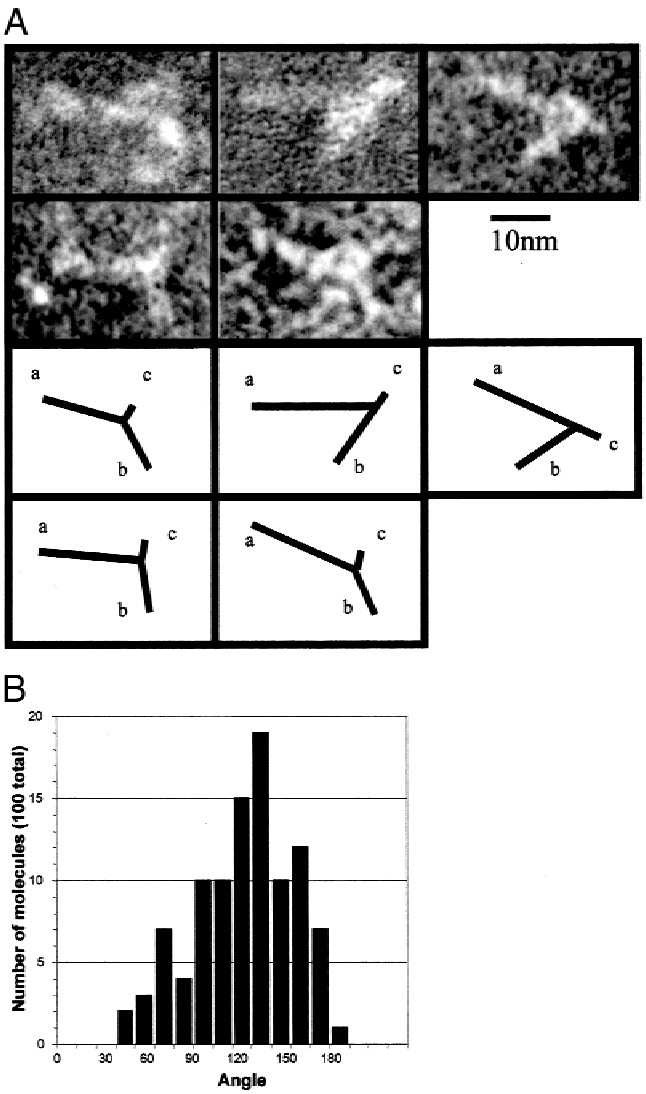

FIGURE 3. HCV IRES. **A:** Electron microscopic images of the HCV IRES molecules with diagrammatic representations of the structures noted. **B:** Angular distribution between stems a and b as labeled above.

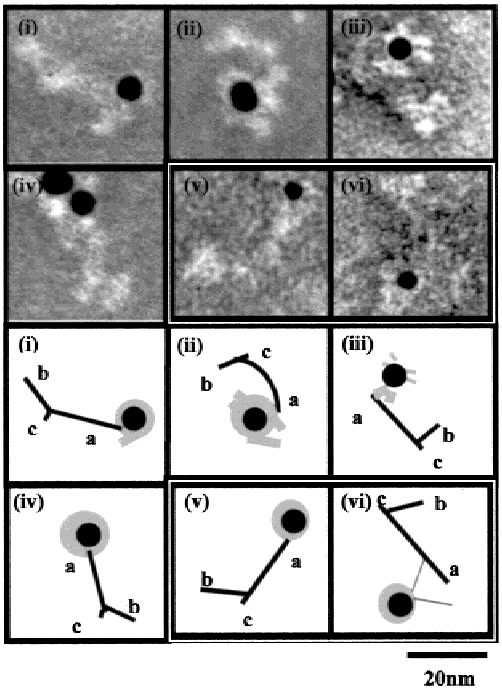

FIGURE 4. Gold labeled HCV IRES. **i–iv**: biotinylated oligonucleotide hybridized to domain IIIb labeled with streptavidin-coated colloidal gold. **v–vi**: Gold labeled PTB bound to the HCV IRES.

rounded by halos of streptavidin with IRES structures attached via the apexes of the longest stem (Fig. 4, i–iv). This both confirmed the identity of the visualized structures and indicated that the 18-nm stem corresponds to domain III of the predicted structure.

Relating observed to predicted structure

To further establish that the visualized structures were HCV IRES elements and to define their orientation, transcripts were coupled by hybridization with tandem repeat oligonucleotides. Initially, an oligonucleotide complementary to the non-base paired region between domains I and II of the IRES was selected as this is predicted to be single stranded and so available for hybridization. Coupled molecules were seen (Fig. 5, i–iv) in which the 10-nm stems (b) were often adjacent to one another. However, because of the flexibility of the region selected for hybridization, a portion of coupled molecules were aligned such that these stems did not meet. This shows that although this oligonucleotide joined the molecules in such a way that the stems b were often brought together, hybridization did not occur at the apex of stem b. Hybridization using oligonucleotide HCEM5 was not performed for the purposes of orientation, but rather to develop the technique and further identify the visualized structures.

A second tandem repeat oligonucleotide was used to hybridize the loop region of domain IIIb. Figure 5, v–vii, shows that molecules were aligned such that the tips of the longest stems (a) were joined. All linked molecules were organized in this way with rotation about the apex of the joined stems resulting from the flexibility of the 10-base spacer between the tandem repeat hybridizing sequences of the oligonucleotide. The alignment of the HCV IRES structures after coupling at domain IIIb confirms that the 18-nm stem is indeed domain III and that a non-base paired region exists at the apex of this domain corresponding to the loop of domain IIIb.

Interaction of PTB with the HCV IRES

PTB has been reported to bind to the HCV IRES, although it is not essential for IRES function. Mixtures of IRES and PTB were examined to obtain direct confirmation of their association and to investigate conformational changes in the IRES that might result from

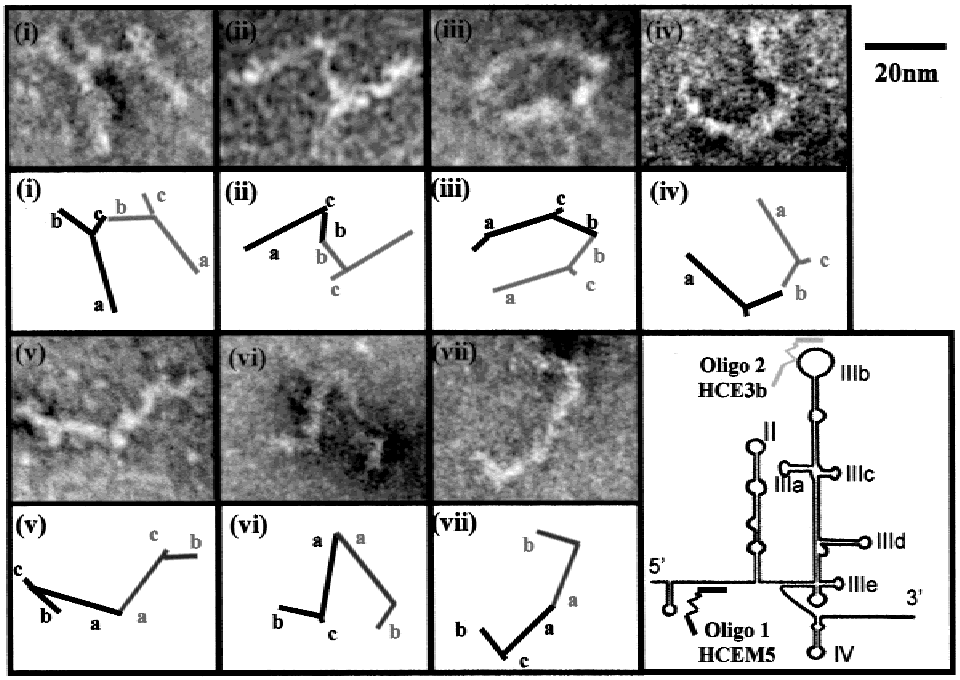

FIGURE 5. Coupled HCV IRES. HCV IRES transcribed in vitro and coupled using tandem repeat oligonucleotides. **i–iv:** coupled at nt 27–41 (5′ end of IRES); **v–vii:** coupled at nt 191–205 (domain IIIb apical loop). After hybridization, RNA was adsorbed to carbon and negatively stained with uranyl acetate.

PTB binding. The polyhistidine-tagged protein was purified using metal-affinity resin to give a single band of the expected size when analyzed by PAGE (Fig. 2C). Binding of the recombinant PTB to the HCV IRES was demonstrated by co-immunoprecipitation of the IRES with PTB using monoclonal antipolyhistidine antibodies and protein G-agarose (Fig. 2D). HCV IRES RNA was removed from the binding mix by antipolyhistidine antibodies coupled to protein G-agarose only in the presence of PTB. When no protein or NS5A (a 56–58-kDa nonstructural protein encoded by HCV) was placed in the binding mix, the HCV IRES remained in solution as co-immunoprecipitation did not occur. Direct visualization of a protein of 57 kDa was difficult, particularly when bound to the IRES, due to the compact nature of the protein in comparison with the HCV IRES. Consequently, we employed an immunogold labeling approach to detect the protein. For this purpose we used an antipolyhistidine antibody that recognized the six-histidine tag that had been linked to the PTB to facilitate purification. This complex was then visualized in the EM using protein A-coated colloidal gold. The binding of PTB was restricted to domain III, the longest stem (Fig. 4, v–vi), one of three PTB binding sites identified by UV crosslinking studies (Fukushi et al., 1997).

Visualization of the FMDV IRES

The HCV IRES differs markedly in size, predicted secondary structure and functional requirements from any of the IRES elements found in picornaviruses. Therefore, we examined by EM RNA transcripts of the IRES domain of a picornavirus, FMDV, to compare its morphology with that of the HCV element. The FMDV IRES was transcribed in vitro and analyzed by polyacrylamide gel electrophoresis (Fig. 2B) prior to negative staining and mounting for EM. As with HCV, the EM grids contained many examples of particles with distinctive structure, although the appearance of these was strikingly different from the HCV IRES. The FMDV structure was larger and had a more complex appearance (Fig. 6A). The long stem measured approximately 35–40 nm and each of the two side stems were 6 nm long. We also examined complexes between the FMDV IRES and PTB (Fig. 6B), which has been shown by biochemical methods to bind to two distinct regions of the sequence (Luz & Beck, 1990; Kolupaeva et al., 1996). Our results confirmed that PTB binds to different sites on the FMDV IRES and its locations on the images allowed us to make a tentative alignment of the predicted structure with the visualized images (Fig. 6D).

DISCUSSION

Negative staining has been successfully used to visualize a highly ordered RNA transcript by electron microscopy. Previous electron microscopic studies of RNA molecules, such as ribozymes, have required the use of polyamines, such as spermidine, to coat the RNA before rotary shadow casting with platinum (Wang et al.,

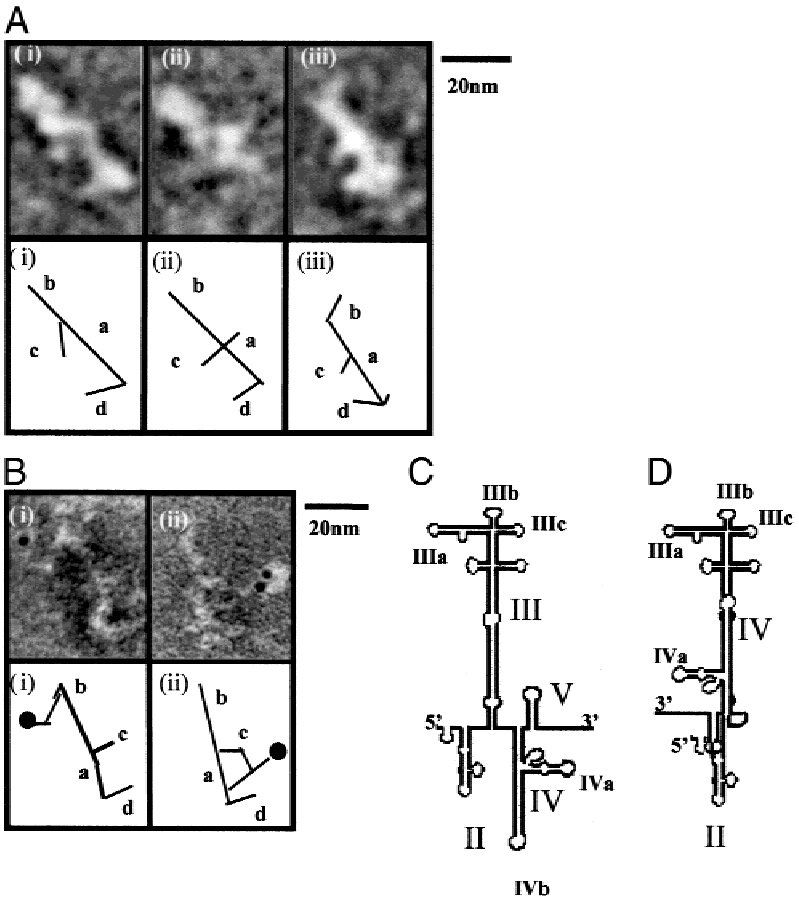

FIGURE 6. FMDV IRES transcribed in vitro. **A:** Negatively stained with 4% uranyl acetate. **B:** Gold-labeled PTB bound to the FMDV IRES. **C:** Map of the FMDV IRES secondary structure. **D:** Predicted alignment of FMDV IRES domains.

1994; Nakamura et al., 1995). However, spermidine has recently been shown to alter the conformation of ribozymes (Walter et al., 1998) and visualization of the HCV IRES in the absence of polyamines removes the uncertainty as to the effects of such agents on the structure of the RNA. Also, negative staining has the advantage over heavy metal shadowing of exhibiting a finer grain size. This technique may be used for the characterization of other large RNA structures and facilitate visualization of the interaction of such molecules with RNA-binding proteins.

The three-stemmed appearance of negatively stained HCV IRES transcripts is in good agreement with the predicted model. It is likely that the three domains visualized represent domains II–IV of the predicted model. Although domain I is included in the construct, it is unlikely that the single-stranded RNA and the very small loop that forms domain I would be seen at the resolution achieved. The extended nature of the RNA domains correlates with the results of small angle X-ray scattering (Kieft et al., 1999), which suggests that the HCV IRES does not form a globular structure. The length of the largest feature, domain III, was estimated by assuming that double-stranded regions of the IRES would adopt A form helices with a 2.73-Å rise per base pair and a 25-Å rise for each laterally protruding double helical subdomain. Using these criteria, domain III was predicted to be $>$16 nm in length. However, the presence of bulges and loops makes accurate prediction of the length of the proposed domain impossible. The 18-nm stem (stem a) seen in the EM images is compatible with domain III.

The second stem (stem b) is 10 nm in length. This fits well with domain II, which was predicted to be at least 7 nm in length. The angles between stems a and b (putative domains III and II) suggests some flexibility, the angle ranging between 70° and 130° with a mean at 95°. A small segment of non-base paired nucleotides in the region joining the stems is likely to be responsible for this ability to rotate. It is worth pointing out that the wide range of angles seen between domains II and III is not a result of varying three-dimensional orientations of the molecules because “out of plane” stems would not be visualized by the negative staining technique. This is in contrast to a study of the *Tetrahymena* group I intron ribozyme by Nakamura et al. (1995) that employed a rotary shadowing technique that does impart contrast to distal segments of a stem that protrudes

away from the support film surface. The latter report also demonstrated flexibility in RNA stems around a pseudoknot hinge.

We have refined the model of the HCV IRES structure based on possible arrangements of domains II and III (Fig. 7). Flexibility may be necessary for interaction of domain III with proteins involved in initiation of translation. Although a recent study shows that subunits of eIF3 can bind to domain III in isolation (Buratti et al., 1998), binding of the ribosomal protein S9 of the 40s ribosomal subunit requires the correct orientation of domains IIa, IIc, and IIId (Oldreman-Macchioli et al., 2000). Thus movement of domain II relative to domain III may be prerequisite for binding of the 40s ribosomal subunit or subsequent events in HCV IRES-mediated initiation of translation. Unfortunately, the small size of the predicted apical loop of domain II precludes the use of oligonucleotides for further characterization of this region of the IRES.

The shortest stem (stem c) seen on the particles is 2 nm long and probably corresponds to domain IV. This region is adjacent to the pseudoknot and the putative ribosomal-binding site. The exact role of this stem in translation initiation is unclear as several studies demonstrate that disruption of the stem loop that forms domain IV has little effect on the efficiency of translation (Tsukiyama-Kohara et al., 1992; Wang et al., 1993). In contrast, certain reporter constructs in which the base pairing of this stem has been disturbed show a marked decrease in expression of the reporter protein (Reynolds et al., 1995; Honda et al., 1996; Lu & Wimmer, 1996). In the latter case, the reporter gene sequence may interact with and disrupt upstream secondary and tertiary RNA structures, thereby altering the conformation of the IRES. It is clear however, that the hinge region between stems a and b is critical for ribosome attachment. Interaction of additional proteins with the upper regions of these stems may stabilize this hinge region and thereby facilitate or regulate internal ribosome entry. Although it is possible that additional domains may not be visualized by negative staining due to out of plane orientation, this is unlikely to be the case because the size of the domains seen correlates well with size and structure of the predicted model.

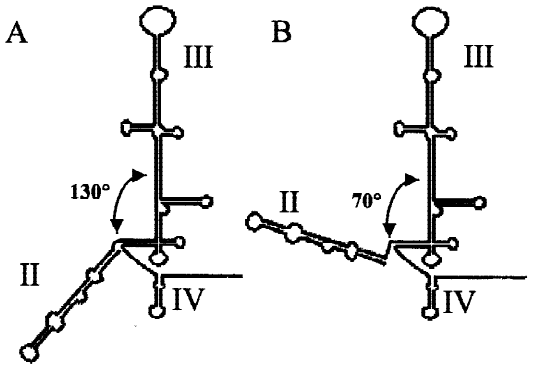

FIGURE 7. Alignment of HCV IRES domains based on EM studies.

Hybridization of the RNA molecules with specific oligonucleotides complementary to predicted single-stranded regions served both to conclusively identify the observed particles as IRES elements and to orient the images with respect to the overall proposed structure. Hybridization with a biotinylated oligonucleotide and visualization with streptavidin-labeled gold particles confirmed that the structures seen were, indeed, IRES elements. Furthermore, hybridization of the IRES RNA with tandem repeat oligonucleotides resulted in dimerization of the particles. From this it can be concluded that the particles are monomeric, because multimeric hybridized aggregates would be seen if each particle was composed of more than one molecule. It was also possible to equate the points of contact of the dimeric structures with the sequences to which the oligonucleotides were complimentary. This approach enabled identification of the domain IIIb loop of the HCV IRES.

PTB is involved in mRNA splicing in eukaryotic cells but has also been shown to be essential for efficient IRES-mediated translation in picornaviruses. Although PTB binding to the HCV IRES has been demonstrated by UV crosslinking and RNase protection, no functional role for this interaction has been demonstrated. Binding of PTB to a region within domain III was clearly demonstrated by using colloidal gold and a specific antibody to label the RNA-binding protein. The HCV IRES contains three polypyrimidine tracts, one at the base of domain II (nt 37–45), a second in the sequence between domains II and III (nt 120–130) and finally in the apical loop of domain III (nt 191–199). UV crosslinking studies confirm the ability of PTB to associate with each of these regions (Ali & Siddiqui, 1995). Our data suggest a preference for binding of PTB to the second polypyrimidine tract of the HCV IRES in domain IIIb.

The picornavirus FMDV has a type II IRES (Fig. 6C) that is larger than that of HCV and has a more complex predicted structure. It also differs from HCV in requiring almost all of the canonical initiation factors, as well as PTB, to initiate translation of the FMDV genome. For comparison with the HCV IRES, the FMDV IRES was also visualized and preliminary data are presented. Although, as expected, the FMDV IRES was larger than and appeared to be structurally distinct from the HCV IRES, the observed size difference was greater than would be predicted from the length of the transcripts. The FMDV IRES RNA is 16% longer than the HCV IRES transcript but appears to be 46–60% larger by EM. However, in the HCV IRES RNA, the first 40 nt upstream of domain II and 40 nt down stream of domain IV are almost entirely single stranded and would therefore be lost to the background with the staining

procedure employed. Thus, only 300 nt of the HCV IRES formed visible structures. In comparison, as there is very little single-stranded RNA in the FMDV IRES transcript, almost the entire 442 nt was visualized, making an estimated size difference of 42%. The presence of a pseudoknot in the HCV RNA would also pull the molecule into a more compact structure than the FMDV IRES.

Orientation of the FMDV IRES is now required to distinguish the stems seen for comparison with the predicted model. The ability to visualize interactions of the FMDV IRES with PTB allows the tentative assignment of domains to stems within the images. Previous studies indicate that PTB binds to two sites on the FMDV IRES, the apical loops of domain II and IVa. It was previously unclear as to whether these two sites formed a single binding domain or were capable of interacting with the protein independently. This study shows that the latter is the case as gold labeling of IRES-bound PTB is seen in two distinct regions of the molecule. We predict that the binding sites in Figure 3B(i) and (ii) correspond to the apical loops of domain II and domain IVa, respectively. If this is the case, it is possible to speculate that the stem a in the FMDV IRES electron micrographs represents domain III with stem d formed by domain IIIa. Domain IV may be rotated such that stem loop IVa forms stem c of the visualized IRES (Fig. 6D).

We show here that negative staining EM techniques can be used to visualize IRES RNAs, which are seen as particles of distinct morphology. Further application of this technique to give low-resolution information on the structure of such RNA segments will aid interpretation of higher resolution data that may be obtained by other biophysical methods such as NMR spectroscopy and X-ray crystallographic analysis of defined domains. NMR spectroscopy has recently been successfully employed to solve the structure of two small domains of the HCV IRES (IIId and IIIe; Klinck et al., 2000; Lukavsky et al., 2000). Examination of additional protein/RNA complexes by EM of negatively stained specimens, combined with the recent advances in cryo-EM that will make possible single-particle reconstruction of the IRES complexed with the ribosome, will also help to provide insights into the structure/function relationships in cellular and virus IRESs.

MATERIALS AND METHODS

HCV IRES template

The template for transcription in vitro, SK-HCV 5′UTR consisted of nucleotides 1–380 of HCV strain N2, genotype 1b (full-length clone of HCV N2 kindly donated by Prof. S. Lemon, University of Texas, Galveston) downstream of a T7 RNA polymerase promoter sequence on a pBluescript SK+ (Stratagene) background. The cloned region of HCV encodes the full 5′UTR as well as the first 39 nt of the core coding region.

Preparation of HCV IRES RNA

Approximately 10 μg SK-HCV5′UTR was transcribed in vitro using 5 μg T7 RNA polymerase in a 100-μL reaction mix containing 80 mM HEPES-KOH, pH 7.5, 24 mM $MgCl_2$, 2 mM spermidine, 40 mM DTT, 7.5 mM each rNTP, 500 U inorganic pyrophosphatase and 4 U ribonuclease inhibitor. The transcription reaction was incubated overnight at 37 °C, after which the template was digested with 10 U RNase free DNase (Promega) for 15 min at 37 °C. The transcribed RNA was purified by phenol chloroform extraction followed by ethanol precipitation and washing. The resuspended RNA was further purified using a Nanosep 10K filter (Flowgen). The integrity of the purified transcripts was determined by electrophoresis on a 6% polyacrylamide, 7 M urea, TBE gel. To ensure correct folding of the IRES, magnesium chloride was added to the RNA to a concentration of 5 mM and the solution heated to 65 °C for 1 min followed by cooling to room temperature for 30 min.

Electron microscopy

After purification and folding, the RNA was diluted to 2.5 μg mL^{-1} ($\sim 10^{14}$ molecules mL^{-1}). The HCV IRES was adsorbed onto a carbon film and negatively stained using an aqueous solution of uranyl acetate (4% w/v, pH 4.25) following essentially a protocol described by Hoppert and Holzenburg (1998). The adsorption time was 30 s followed by a wash in double-distilled water for 10 s and incubation on 4% uranyl acetate for 1 min. Specimens were then mounted onto copper grids (400 mesh) and blotted dry. Micrographs were recorded on Agfa Scientia 23D56 electron image sheet films at calibrated magnifications in a Philips CM10 transmission electron microscope operated at 100 kV.

Steptavidin-gold labeling

The HCV IRES was hybridized with a biotinylated oligonucleotide specific to the loop region of domain IIIb, which was then labeled with streptavidin-coated gold particles. A 150-μL droplet of the HCV IRES (2.5 μg mL^{-1} in 50 mM Tris HCl, pH 8.0, 10 mM $MgCl_2$), prepared as above, was overlaid with 10 μL of the biotinylated oligonucleotide ($\sim 10^{15}$ molecules mL^{-1}; biotin-5′-TTATCCAAGAAAGG-3′). After 1 min, 10 nm streptavidin-coated gold particles were added. The mix was adsorbed onto carbon film and stained as previously described.

Coupling of IRES molecules

Tandem repeat oligonucleotides (Table 1) were used to couple HCV IRES molecules. The RNA droplet prepared as above was overlaid with 10 μL of the appropriate oligonucleotide and incubated for 1 min prior to staining and mounting (see above).

PTB binding

His-tagged PTB was expressed in *Escherichia coli* SG13009 cells using a construct kindly donated by S. Curry (Imperial College, London). The expressed protein was purified using TALON metal-affinity resin according to the manufacturer's

TABLE 1. Tandem repeat oligonucleotides.

Oligonucleotide	Sequence	Site of hybridization
HCEM5	5′-GTGATCTATGGTGGAAAAAAAAGTGATCTATGGTGG-3′	nt 27–41
HCEM3b	5′-TGATCCAAGAAAGGAAAAAAAATGATCCAAGAAAGG-3′	domain IIIb, nt 191–205

instructions. Briefly, PTB was solubilized by sonication in lysis buffer (20 mM Tris HCl, pH 7.6, 250 mM NaCl) + 0.1% Triton X-100. The cleared lysate was added to the TALON resin and incubated 1 h at room temperature with gentle rocking. The resin was washed in lysis buffer containing 10 mM imidazole and PTB eluted in lysis buffer + 100 mM imidazole.

To demonstrate binding of the HCV IRES to the purified His-tagged PTB, an co-immunoprecipitation of the IRES bound to PTB was performed. As a negative control, His-tagged HCV NS5A was also incubated with the IRES and immunoprecipitated. In each case, 5 μg of protein (PTB or NS5A) was incubated with 2.5 μg HCV IRES in 40 mM HEPES-KOH, pH 7.5, 35 mM NaCl, 12 mM $MgCl_2$ for 1 h at room temperature. Antipolyhistidine antibodies (Sigma) were incubated with protein G-agarose (Sigma) for 1 h at 4 °C. The agarose was pelleted by centrifugation and resuspended in the above protein–IRES binding mix. The resulting mix was incubated at room temperature for 1 h, after which the protein G-agarose was pelleted and the supernatant removed for analysis by native polyacrylamide-TBE gel electrophoresis.

Protein A-coated colloidal gold (5 nm spheres; Sigma) was diluted 1:100 in 20 mM Tris HCl, pH 7.5, 50 mM NaCl and antipolyhistidine antibodies were added to a concentration of 200 ng mL^{-1} and incubated for 30 min at room temperature. Purified PTB was then added to 4 μg mL^{-1} and HCV IRES transcripts to 5 μg mL^{-1}. The mixture was then incubated a further 30 min at room temperature. Samples were then prepared for electron microscopy as described above.

Preparation and visualization of the FMDV IRES

The IRES (442 nt immediately preceding the initiation codon) of FMDV strain A10 was also cloned into a Bluescript SK vector and transcribed in vitro as detailed above. Transcripts were purified and prepared for TEM as previously described. PTB binding and visualization by immunolabeling and EM were carried out as described above for the HCV IRES.

ACKNOWLEDGMENTS

We thank S. Lemon and S. Curry for the provision of HCV IRES and PTB clones, respectively, A. Macdonald for recombinant His-tagged NS5A, and A. Hick and P. McPhie for technical support in electron microscopy. This work was funded by Biotechnology and Biological Sciences Research Council project grant 24-B11731.

Received July 17, 2000; returned for revision August 25, 2000; revised manuscript received January 22, 2001

REFERENCES

Ali N, Siddiqui A. 1995. Interaction of polypyrimidine tract-binding protein with the 5′ noncoding region of the hepatitis C virus RNA genome and its functional requirement in internal initiation of translation. *J Virol 69*:6367–6375.

Ali N, Siddiqui A. 1997. The La antigen binds 5′ noncoding region of the hepatitis C virus RNA in the context of the AUG codon and stimulates internal ribosome entry site-mediated translation. *Proc Natl Acad Sci USA 94*:2249–2254.

Ban N, Nissen P, Hansen J, Moore PB, Steitz TA. 2000. The complete atomic structure of the large ribosomal subunit at 2.4 Å resolution. *Science 289*:905–920.

Belsham GJ, Brangwyn JK. 1990. A region of the 5′ noncoding region of foot-and-mouth disease virus RNA directs efficient internal initiation of protein synthesis within cells: Involvement with the role of L-protease in translational control. *J Virol 64*:5389–5395.

Borman A, Howell MT, Patton JG, Jackson RJ. 1993. The involvement of a spliceosome component in internal initiation of human rhinovirus RNA translation. *J Gen Virol 74*:1775–1788.

Borvjagin AV, Pestova TV, Shatsky IN. 1994. Pyrimidine tract binding protein strongly stimulates in vitro encephalomyocarditis virus RNA translation at the level of the preinitiation complex formation. *FEBS Lett 351*:299–302.

Brown EA, Zhang H, Ping LH, Lemon SM. 1992. Secondary structure of the 5′ non-translated regions of hepatitis C virus and pestivirus genomic RNAs. *Nucleic Acids Res 20*:5041–5045.

Buratti E, Tisminetzky S, Zotti M, Baralle FE. 1998. Functional analysis of the interaction between HCV 5′ UTR and putative subunits of eukaryotic translation initiation factor eIF3. *Nucleic Acids Res 26*:3179–3187.

Cate JH, Gooding AR, Podell E, Zhou K, Golden BL, Kundrot CE, Cech TR, Doudna JA. 1996. Crystal structure of a group I ribozyme domain; principles of RNA packing. *Science 273*:1678–1685.

Chiu CY, Cary RB, Chen DJ, Peterson SR, Stewart PL. 1998. Cryo-EM imaging of the catalytic subunit of the DNA-dependent protein kinase. *J Mol Biol 184*:1075–1081.

Fukushi S, Kurihara C, Ishiyama N, Hoshino FB, Oya A, Katayama K. 1997. The sequence element of the internal ribosome entry site and a 25-kilodalton cellular protein contribute to efficient internal initiation of translation of hepatitis C virus RNA. *J Virol 71*:1662–1666.

Glass MJ, Jia XY, Summers DF. 1993. Identification of hepatitis A virus internal ribosome entry site: In vivo and in vitro analysis of bicistronic RNAs containing the HAV 5′ noncoding region. *Virology 193*:842–852.

Haley DA, Bova MP, Huang Q-L, Mchaourab HS, Stewart PL. 2000. Small heat-shock protein structures reveal a continuum from symmetric to variable assemblies. *J Mol Biol 298*:261–272.

Hellen CUT, Witherell GW, Schmid M, Shin SH, Pestova TV, Gil A, Wimmer E. 1993. A cytoplasmic 57-kDa protein that is required for initiation of translation is identical to the nuclear pyrimidine tract binding protein. *Proc Natl Acad Sci USA 90*:7642–7646.

Honda M, Beard MR, Ping L-H, Lemon SM. 1999a. A phylogenetically conserved stem-loop structure at the 5′ border of the internal ribosome entry site of hepatitis C virus is required for cap-independent viral translation. *J Virol 73*:1165–1174.

Honda M, Ping L-H, Rijnbrand R, Amphlett E, Clark B, Rowlands D, Lemon SM. 1996. Structural requirements for initiation of translation by internal ribosome entry within genome-length hepatitis C virus RNA. *Virology 222*:31–42.

Honda M, Rijnbrand R, Abell J, Kim D, Lemon SM. 1999b. Natural variation in translational activities of the 5′ nontranslated RNAs of hepatitis C virus genotypes 1a and 1b: Evidence for long-range

RNA–RNA interaction outside of the internal ribosomal entry site. *J Virol 73*:4941–4951.
Hoppert M, Holzenburg A. 1998. *Electron microscopy in microbiology; RMS handbook,* Vol 35. Bios Scientific, Oxford.
Jang SK, Davies MV, Kaufman RJ, Wimmer E. 1989. Initiation of protein synthesis by internal entry of ribosomes into the 5′ nontranslated region of encephalomyocarditis virus RNA in vivo. *J Virol 631*:1651–1660.
Jang SK, Krausslich H-G, Nicklin MJH, Duke GM, Palmenburg AC, Wimmer E. 1988. A segment of the 5′ nontranslated region of encephalomyocarditis virus RNA directs internal entry of ribosomes during in vitro translation. *J Virol 62*:2636–2643.
Kaminski A, Hunt SL, Gibbs CL, Jackson RJ. 1994. Internal initiation of mRNA translation in eukaryotes. In: Setlow J, ed. *Genetic engineering: Principles and methods*, Vol 16. New York: Plenum. pp 115–155.
Kaminski A, Hunt SL, Patton JG, Jackson RJ. 1995. Direct evidence that polypyrimidine tract binding protein (PTB) is essential for internal initiation of translation of encephalomyocarditis virus RNA. *RNA 1*:924–938.
Kieft JS, Zhou K, Jubin R, Murray MG, Lau, JYN, Doudna JA. 1999. The hepatitis C virus internal ribosome entry site adopts an ion-dependent tertiary fold. *J Mol Biol 292*:513–529.
Kim SH, Suddath FL, Quigley GJ, McPherson A, Sussman JL, Wang AHJ, Seeman NC, Rich A. 1974. Three dimensional tertiary structure of yeast phenylalanine transfer RNA. *Science 185*:435–440.
Klinck R, Westhof E, Walker S, Afshar M, Collier A, Abou-ela F. 2000. A potential RNA drug target in the hepatitis C virus internal ribosome entry site. *RNA 6*:1423–1431.
Kolupaeva VG, Hellen CUT, Shatsky IN. 1996. Functional analysis of the interaction of the pyrimidine tract binding protein with the internal ribosomal entry site of encephalomyocarditis virus and foot-and-mouth disease virus RNAs. *RNA 2*:1199–1212.
Kozak M. 1989. The scanning model for translation: An update. *J Cell Biol 108*:229–241.
Lu HH, Wimmer E. 1996. Poliovirus chimeras replicating under the translational control of genetic elements of hepatitis C virus reveal unusual properties of the internal ribosome entry site of hepatitis C virus. *Proc Natl Acad Sci USA 93*:1412–1417.
Lukavsky PJ, Otto GA, Lancaster AM, Sarnow P, Puglisi JD. 2000. Structures of two RNA domains essential for hepatitis C virus internal ribosome entry site function. *Nat Struct Biol 7*:1105–1110.
Luz N, Beck E. 1990. A cellular 57 kDa protein binds two regions of the internal translation initiation site of foot-and-mouth disease virus. *FEBS Lett 269*:311–314.
Macejack DG, Sarnow P. 1991. Internal initiation of translation mediated by the 5′ leader of a cellular mRNA. *Nature 353*:90–94.
Meerovitch K, Pelletier J, Sonenberg N. 1989. A cellular protein that binds to the 5′ noncoding region of poliovirus RNA: Implications for internal translation initiation. *Genes & Dev 3*:1026–1034.
Meerovitch K, Svitkin YV, Lee HS, Lejbkowicz F, Kenan DJ, Chan EK, Agol VI, Keene JD, Sonenberg N. 1993. In vitro mutation analysis of *cis*-acting RNA translation elements within poliovirus type 2 5′-untranslated region. *J Virol 67*:3798–3807.
Nakamura TM, Wang Y-H, Zaug AJ, Griffith JD, Cech TR. 1995. Relative orientation of RNA helices in a group I ribozyme determined by helix extension electron microscopy. *EMBO J 14*:4849–4859.
Niepmann M, Petersen A, Meyer K, Beck E. 1997. Functional involvement of polypyrimidine tract-binding protein in translation initiation complexes with the internal ribosome entry site of foot-and-mouth disease virus. *J Virol 71*:8330–8339.
Nissen P, Hansen J, Ban N, Moore PB, Steitz TA. 2000. The structural basis of ribosome activity in peptide bond synthesis. *Science 289*:920–930.
Oldreman-Macchioli FE, Tisminetzky S, Zotte M, Baralle FE, Buratti E. 2000. Influence of correct secondary and tertiary RNA folding on the binding of cellular factors to the HCV IRES. *Nucleic Acids Res 28*:875–885.
Pelletier J, Sonenberg N. 1988. Internal initiation of translation of eukaryotic mRNA by a sequence derived from poliovirus RNA. *Nature (London) 334*:320–325.
Pelletier J, Sonenberg N. 1989. Internal binding of eukaryotic ribosomes on poliovirus RNA: Translation in HeLa cell extracts. *J Virol 63*:441–444.
Pestova TV, Shatsky IN, Fletcher SP, Jackson RJ, Hellen CUT. 1998. A prokaryotic like mode of cytoplasmic eukaryotic ribosome binding to the initiation codon during internal translation initiation of hepatitis C and classical swine fever virus RNAs. *Genes & Dev 12*:67–83.
Pestova TV, Shatsky IN, Hellen CUT. 1996. Functional dissection of eukaryotic initiation factor 4F: The 4A subunit and the central domain of the 4G subunit are sufficient to mediate internal entry of 43S preinitiation complexes. *Mol Cell Biol 16*:6870–6878.
Poole TL, Wang C, Popp RA, Potgieter LND, Siddiqui A, Collett MS. 1995. Pestivirus translation initiation occurs by internal ribosome entry. *Virology 206*:750–754.
Reynolds JE, Kaminski A, Kettinin H, Carroll AR, Rowlands DJ, Jackson RJ. 1995. Unique features of internal initiation of hepatitis C virus RNA translation. *EMBO J 14*:6010–6020.
Rijnbrand R, Bredenbeek P, van der Stratten T, Whetter L, Inchaupse G, Lemon S, Spaan W. 1995. Almost the entire 5′ non-translated region of hepatitis C virus is required for cap-independent translation. *FEBS Lett 365*:115–119.
Robertus JD, Ladner JE, Finch JT, Rhodes D, Brown RS, Clark BF, Klug A. 1974. Structure of yeast phenylalanine tRNA at 3 Å resolution. *Nature 250*:546–551.
Schluenzen F, Tocilj A, Zarivach R, Harms J, Gluehmann M, Janell D, Bashan A, Bartels H, Agmon I, Franceschi F, Yonath A. 2000. Structure of functionally activated small ribosomal subunit at 3.3 angstroms resolution. *Cell 102*:615–623.
Sizova DV, Kolupaeva VG, Pestova TV, Shatsky IN, Hellen CUT. 1998. Specific interaction of eukaryotic translation initiation factor 3 with the 5′ nontranslated regions of hepatitis C virus and classical swine fever virus RNAs. *J Virol 72*:4775–4782.
Smith DB, Mellor J, Jarvis LM, Davidson F, Kohlberg J, Urdea M, Yap P-L, Simmonds P, and the International HCV Collaborative Study Group. 1995. Variation of the hepatitis C virus 5′ non-coding region: Implications for secondary structure, virus detection and typing. *J Gen Virol 76*:1749–1761.
Tsukiyama-Kohara K, Iizuka N, Kohara M, Nomoto A. 1992. Internal ribosome entry site within hepatitis C virus RNA. *J Virol 66*:1476–1483.
Vagner S, Gensac MC, Maret A, Bayard F, Amalric F, Prats H, Prats AC. 1995. Alternative translation of human fibroblast growth factor 2 mRNA occurs by internal entry of ribosomes. *Mol Cell Biol 15*:35–44.
Wahl MC, Sundaralingam M. 1995. New crystal structures of nucleic acids and their complexes. *Curr Opp Struct Biol 5*:282–295.
Walter F, Murchie AIH, Thomson JB, Lilley DMJ. 1998. Structure and activity of the hairpin ribozyme in its natural junction conformation: Effect of metal ions. *Biochemistry 37*:14195–14203.
Wang C, Sarnow P, Siddiqui A. 1993. Translation of human hepatitis C virus in cultured cells is mediated by an internal ribosome-binding mechanism. *J Virol 67*:3338–3344.
Wang Y-H, Murphy FL, Cech TR, Griffith JD. 1994. Visualization of a tertiary structural domain of the tetrahymena group I intron by electron microscopy. *J Mol Biol 236*:65–71.